VOL. 18, NO. 7, APRIL 2023 ISSN 1819-6608
ARPN Journal of Engineering and Applied Sciences

www.arpnjournals.com

A COMPARISON STUDY BETWEEN THE OPTIMAL DFIG FLUX AND SPEED CONTROL IN THE PRESENCE OF MAGNETIC HYSTERESIS AND CLASSICAL CONTROL STRATEGIES FOR WIND SYSTEMS

A. Barra[1], A. Moutabir[1], H. Ouadi[2] and B. Bensassi[1]
[1]GEITIIL Lab, University Hassan II, Faculty of Science, Casablanca, Morocco
[2]ERERA Lab, ENSAM, Mohammed V University, Rabat, Morocco
E-Mail: barra.adil@Gmail.com

ABSTRACT

In the wind energy systems field, the most common control objective treated by authors is the speed and flux control of the doubly fed induction generator (DFIG). For computing complexity matter, the generator mathematical representation is generally modelled assuming a linear magnetic characteristic. Based on this assumption, the rotor flux control will aim to track a fixed flux reference, mostly its nominal value. The inconvenience with this strategy is that practically, neglecting the nonlinearity of the generator's magnetic characteristic, optimal performance control cannot be performed. In this study, considering the magnetic flux hysteresis and saturation characteristic, new modelling of the DFIG is presented. Furthermore, a new speed and optimal flux Backstepping controller is designed based on the Lyapunov theory. To prove its performance, a comparison study with different control strategies will be conducted. Simulations considering a wide range of wind speed variations are illustrated in the Matlab/Simulink environment.

Keywords: wind turbines, DFIG, MPPT, Hysteresis, backstepping control.

Manuscript Received 14 December 2022; Revised 12 May 2023; Published 30 May 2023

1. INTRODUCTION

In the few last decades, renewable energies including wind turbines got major attention worldwide. Regardless there epic performances, wind turbines based on DFIG are complex, and their control law design is difficult [7] since the considered model is multivariable and highly nonlinear.

The control of the DFIG using linear or nonlinear controllers has been the subject of several earlier studies [6-10]. The speed tracking objective and flux regulation for MPPT is the most treated subject present in the literature. However, the proposed controllers function as intended when a linear magnetic characteristic is assumed. Practically, this assumption is not realistic [3, 4, 5], as the DFIG magnetic characteristic is non-linear and manifests unfavourable errors and oscillations [15] due to the hysteresis and saturation phenomenon produced by the magnetic material. However, if the rotor flux regulation is done in the vicinity of a constant nominal value, standard models (ignoring the magnetic non-linearity) can still be employed in speed control design. Only when the aerodynamic torque is near the nominal DFIG electromagnetic torque value, it's exclusively in this scenario that the DFIG efficiency reaches its maximum. However, the aerodynamic torque is typically not a priori fixed and may be subject to large range variation in real applications, due to the considerable variance in wind speed.

To address the aforementioned issues, a new speed control system, using online rotor flux reference adjustment to track the optimal speed reference in the presence of significant wind speed variation must be developed. The optimal flux reference will also experience considerable range variations under these circumstances, signifying considerable excursions of the operating point on the magnetic characteristic. Therefore, the controller design should be based on a model that takes into consideration the nonlinearity of the machine's magnetic circuit to provide high control performances regardless of the DFIG operation mode. Hysteresis and saturation both characterize this nonlinearity

To our knowledge, no paper has dealt yet with the MPPT control of the DFIG under saturation/hysteresis phenomena. In [12]-[13], nonlinear controllers were developed for a wind system by taking only into account the magnetic saturation (neglecting the hysteresis effect). This assumption facilitates relatively the development of the DFIG model and the MPPT regulator synthesis. However, in practice, the hysteresis phenomena degrade the expected wind system performances (problems of precision and oscillations).

Many hysteresis mathematical models were developed to describe the hysteresis phenomena. They can be classified as follows:

a) Operator-based hysteresis models such as the Preisach model and Prandtl-Ishlinskii model, where an infinite number of hysteretic operators are involved in their integral model which implies high computation complexities [3].

b) Differential equation-based hysteresis models such as the Backlash-like model, Bouc-Wen model, or Duhem model, where the finite number of hysteretic operators can be easily extended to continuous inputs by using approximation and a limiting process, avoiding the computation complexity [3].

In the present work, a special case of the Duhem model, the Coleman-hudgdon model [2] is considered to describe the magnetic nonlinear characteristic. This model

ARPN Journal of Engineering and Applied Sciences

proved to be quite convenient for hysteresis modelling in ferromagnetic materials [2, 14].

The nonlinearity of the magnetic characteristic will be taken into account when a revised model for the DFIG is built in this paper. Furthermore, a new controller for the considered wind system is developed based on this new model. The two control objectives are as follows: *i)* tracking the optimal reference of the DFIG's rotor speed (for an MPPT purpose); *ii)* tracking the optimal reference of the DFIG's rotor flux. The optimization of the rotor flux implies the minimization of the stator current, which will reduce the stator's joule losses. The DFIG speed/flux controller created using the backstepping technique turns out to be very different from the conventional DFIG control strategies that consider a constant flux references and assume a linear magnetic characteristics. Despite variations in wind speed, the newly developed controller is formally demonstrated to be globally asymptotically stable and enforces the speed and flux to exactly trace their fluctuating reference trajectory.

To highlight the interest in taking account of the saturation/hysteresis phenomena in the control design, the performances of a classical regulator (neglecting the saturation/hysteresis) will be evaluated by simulation, concerning those of the new proposed controller. On the other hand, for checking the robustness of the proposed wind turbine system, the controller performances will be inspected in the presence of different electrical grid faults (Voltages dips, frequency deviation, and load variation)

This paper is organized as follows: Section 2 describes the characterisation of magnetic hysteresis in induction machines. Section 3 describes the induction machine model; the machine speed/flux controller is designed and analyzed in Section 4; the controller performances are illustrated by simulations in Section 5.

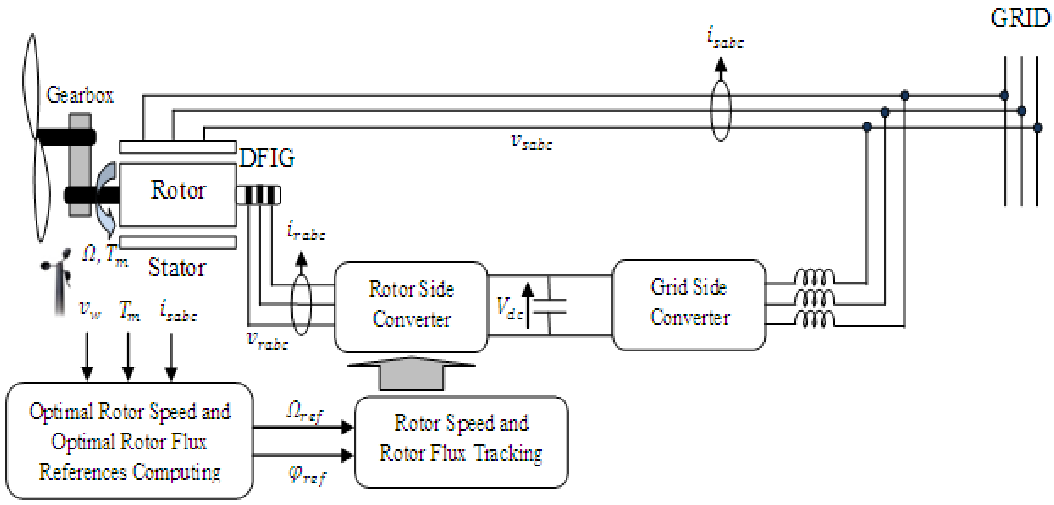

Figure-1. General schema of the considered wind system.

Table-1. Notations and symbols.

p	**Poles pairs**
Ω	DFIG rotor speed
$V_{s\alpha}, V_{s\beta}$	Stator voltage (α-β) components
$V_{r\alpha}, V_{r\beta}$	Rotor voltage (α-β)components
V_{sd}, V_{sq}	Stator voltage in (d-q) rotating frame
J, f	Total inertia constant, Friction ratio
L_s, L_r	Stator, Rotor cyclic induction
M_{sr}	Mutual cyclic induction
R_s, R_r	Stator, Rotor resistance(per phase)
ω_s, ω	Stator, Rotor pulsation
$i_{r\alpha}, i_{r\beta}$	Rotor current (α-β) components
$i_{s\alpha}, i_{s\beta}$	Stator current (α-β) components
$i_{\mu\alpha}, i_{\mu\beta}$	The magnetizing current (α-β) components
$\varphi_{r\alpha}, \varphi_{r\beta}$	Rotor flux (α-β) components
$\varphi_{s\alpha}, \varphi_{s\beta}$	Stator flux (α-β) components
$\varphi_{\mu\alpha}, \varphi_{\mu\beta}$	The magnetizing flux (α-β) components
T_m	Electromagnetic Torque
T_L	Load Torque
R	Radius of the turbine
ρ	Air density
σ	Dispersion ratio
Ω_{ref}	Rotor speed reference
φ_{ref}	Rotor flux reference
P_a	Aerodynamic power
$C_P(\lambda)$	Power coefficient
v_w	Wind speed
V_{smax}	The norm of the stator voltage

2. CHARACTERISATION OF MAGNETIC HYSTERESIS-SATURATION IN AC MACHINES

The Coleman-Hodgdon model comes from the duhem model, which was proposed for active hysteresis in 1897 [2]. Using a phenomenological approach, this differential equation-based hysteresis model focuses on the fact that the output can only change its character when the input changes direction. In this section, the Coleman-Hodgdon model and its properties are introduced briefly [1].

A differential model for hysteresis can be represented by the duhem hysteresis model. Duhem's magnetic hysteresis model has been thoroughly studied by Coleman and Hodgdon. For ease of use, this type of duhem model will be referred to as the CH model throughout this study [1]. It can be represented in terms of the CH model as:

$$\frac{d\varphi_\mu}{dt} = \frac{1}{2}\Big(g_1(i_\mu,\varphi_\mu) - g_2(i_\mu,\varphi_\mu)\Big)\left|\frac{di_\mu}{dt}\right| + \frac{1}{2}\Big(g_1(i_\mu,\varphi_\mu) - g_2(i_\mu,\varphi_\mu)\Big)\frac{di_\mu}{dt}, \forall t \in (0,T) \quad (1)$$

$$\varphi_\mu(0) = \varphi_{\mu 0} \quad (2)$$

Where

$$g_1 = g(i_\mu) + \alpha\big(f(i_\mu) - \varphi_\mu\big) \quad (3)$$

$$g_2 = g(i_\mu) - \alpha\big(f(i_\mu) - \varphi_\mu\big) \quad (4)$$

Introducing (3), (4) into (1), one has:

$$\frac{d\varphi_\mu}{dt} = \alpha\left|\frac{di_\mu}{dt}\right|\big[f(i_\mu) - \varphi_\mu\big] + \frac{di_\mu}{dt}g(i_\mu) \quad (5)$$

with α a positive constant, and the three following conditions are to be satisfied.

Condition 1: $f(.)$ is piecewise smooth, monotone increasing, with $\lim_{i_\mu\to\infty} f'(i_\mu)$ finite;

Condition 2: $g(.)$ is piecewise continuous, even, with $\lim_{i_\mu\to\infty} g(i_\mu) = \lim_{i_\mu\to\infty} f'(i_\mu)$

Condition 3: For all $i_\mu > 0,\ f'(i_\mu) > g(i_\mu) > \alpha e^{\alpha i_\mu}\int_{i_\mu}^{\infty}|f'(\zeta) - g(\zeta)|e^{-\alpha\zeta}\,d\zeta$

To illustrate the previously studied case for the generator considered in this paper, the corresponding functions $f(.), g(.)$ of the C-H model is chosen as:

$$f(i_\mu) = c\tanh(i_\mu) + ai_\mu \quad (6)$$

$$g(i_\mu) = f'(i_\mu)\big(1 - be^{-|i_\mu|}\big) \quad (7)$$

Note that the $f(.)$ and $g(.)$ functions respect the three conditions previously presented. Experimental measurements of the magnetic characteristic can be used to calculate the c and α parameters. The chosen values for the studied machine instance are. The adopted values for the case of the machine study are $a = 0.001$, $c = 1.2$, $b = 0.6$ and $\alpha = 3$ (see [1]). The shape of the obtained hysteresis cycle is presented in Figure-2.

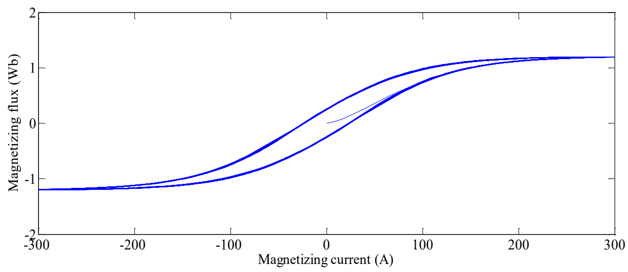

Figure-2. Hysteresis curve is given by the C-H model for the first phase.

3. DOUBLY FED INDUCTION GENERATOR MODEL

A. Electrical and Flux Equations for the AC Machines

The Doubly fed induction generator can be modelled by its electrical and mechanical equations. A stationary reference mark (α, β) will be used to elaborate the control model given in this study. The equations for the AC electrical machine are provided by:
Stator electrical equations [9]

$$V_{s\alpha} = R_s i_{s\alpha} + \frac{d\varphi_{s\alpha}}{dt} \quad (8)$$

$$V_{s\beta} = R_s i_{s\beta} + \frac{d\varphi_{s\beta}}{dt} \quad (9)$$

Rotor electrical equations [9]

$$V_{r\alpha} = R_r i_{r\alpha} + \frac{d\varphi_{r\alpha}}{dt} + \omega\varphi_{r\beta} \quad (10)$$

$$V_{r\beta} = R_r i_{r\beta} + \frac{d\varphi_{r\beta}}{dt} - \omega\varphi_{r\alpha} \quad (11)$$

Likewise, the (α,β) components of the stator and rotor flux verify [9]:

$$\varphi_{s\alpha} = L_s i_{s\alpha} + \varphi_{\mu\alpha} \quad (12)$$

$$\varphi_{s\beta} = L_s i_{s\beta} + \varphi_{\mu\beta} \quad (13)$$

$$\varphi_{r\alpha} = \varphi_{\mu\alpha} \quad (14)$$

$$\varphi_{r\beta} = \varphi_{\mu\beta} \quad (15)$$

the (α, β) components of the magnetizing currents verify:

$$i_{r\alpha} = i_{\mu\alpha} - i_{s\alpha} \quad (16)$$

$$i_{r\beta} = i_{\mu\beta} - i_{s\beta} \quad (17)$$

The classical state-space model of the DFIG is generally presented with this vector

ARPN Journal of Engineering and Applied Sciences

$X = [i_{s\alpha}, i_{s\beta}, \varphi_{r\alpha}, \varphi_{r\beta}, \Omega]^T$ [11], but to introduce the hysteresis character in the state space model, the vector X will be increased by the (α, β) components of the magnetizing current i_μ. The new state vector considered is given by:

$$X = [i_{s\alpha}, i_{s\beta}, \varphi_{r\alpha}, \varphi_{r\beta}, \Omega, i_{\mu\alpha}, i_{\mu\beta}]^T \quad (18)$$

B. Rotor Flux State Equations

The dynamics of the fluxes in the rotor are given by the equations (10) - (11). However, they involve the components (α, β) of the rotor current. These latter are not considered state variables (see 18). We will try to express them according to the components of the vector X.

Indeed, by substituting (16)-(17) in (10)-(11), one obtains the state equations of the rotor fluxes.

$$\frac{d\varphi_{r\alpha}}{dt} = V_{r\alpha} - R_r i_{\mu\alpha} + R_r i_{s\alpha} - \omega\varphi_{r\beta} \quad (19)$$

$$\frac{d\varphi_{r\beta}}{dt} = V_{r\beta} - R_r i_{\mu\beta} + R_r i_{s\beta} + \omega\varphi_{r\alpha} \quad (20)$$

C. Stator Current State Equations

By introducing (12) - (13) in (8) - (9), we deduce the dynamics of the currents in the stator:

$$\frac{di_{s\alpha}}{dt} = -\frac{R_s}{L_s} i_{s\alpha} + \frac{1}{L_s} V_{s\alpha} - \frac{1}{L_s}\frac{d\varphi_{\mu\alpha}}{dt} \quad (21)$$

$$\frac{di_{s\beta}}{dt} = -\frac{R_s}{L_s} i_{s\beta} + \frac{1}{L_s} V_{s\beta} - \frac{1}{L_s}\frac{d\varphi_{\mu\beta}}{dt} \quad (22)$$

Since the components (α, β) of the magnetic flux are not considered as state variables, then, by introducing (14) - (15), (16) - (17) in (19) - (20), one obtains:

$$\frac{di_{s\alpha}}{dt} = -\frac{R_s}{L_s} i_{s\alpha} + \frac{1}{L_s} V_{s\alpha} - \frac{1}{L_s}\left[V_{r\alpha} - R_r i_{\mu\alpha} + R_r i_{s\alpha} - \omega\varphi_{r\beta}\right] \quad (23)$$

$$\frac{di_{s\beta}}{dt} = -\frac{R_s}{L_s} i_{s\beta} + \frac{1}{L_s} V_{s\beta} - \frac{1}{L_s}\left[V_{r\beta} - R_r i_{\mu\beta} + R_r i_{s\beta} + \omega\varphi_{r\alpha}\right] \quad (24)$$

D. State Equations of the Rotor Speed

The electromagnetic torque T_m delivered by the generator is given by [9]:

$$T_m = p(\varphi_{s\alpha} i_{s\beta} - \varphi_{s\beta} i_{s\alpha}) \quad (25)$$

By using the flux equations (12) - (13), the electromagnetic torque can be expressed in function of the (α, β) components of the rotor flux (considered as state variables), namely:

$$T_m = p(\varphi_{r\alpha} i_{s\beta} - \varphi_{r\beta} i_{s\alpha}) \quad (26)$$

While applying the rotation dynamics principle, one deducts the rotor speed state equation

$$\frac{d\Omega}{dt} = \frac{p}{J}(\varphi_{r\alpha} i_{s\beta} - \varphi_{r\beta} i_{s\alpha}) - \frac{T_L}{J} - \frac{f}{J}\Omega \quad (27)$$

E. Magnetizing Current State Equations

Recall that taking into account the hysteresis is carried out by the C-H model defined in (5). This latter expressed the dynamic of the magnetizing flux. By convenience, this model is taken again in this paragraph

$$\frac{d\varphi_{\mu k}}{dt} = \frac{di_{\mu k}}{dt}\left(\alpha sign(\dot{i}_{\mu k})[f(i_{\mu k}) - \varphi_{\mu k}] + g(i_{\mu k})\right) \quad (28)$$

where k=1,2,3 represents the different phases. Otherwise, it is easily checked (by referring to the hysteresis cycle Figure-2), that the variation sense of the current $i_{\mu k}$ is identical to the variation sense of the flux $\varphi_{\mu k}$. Accordingly, one has

$$sign(\dot{i}_{\mu k}) = sign(\dot{\varphi}_{\mu k}) \quad (29)$$

Let's define h as the quantity

$$h(i_{\mu k}, \varphi_{\mu k}, i_{\mu k}) = \frac{1}{(\alpha sign(i_{\mu k})[f(i_{\mu k}) - \varphi_{\mu k}] + g(i_{\mu k}))} \quad (30)$$

where

$$\frac{di_{\mu k}}{dt} = h(i_{\mu k}, \varphi_{\mu k}, i_{\mu k})\frac{d\varphi_{\mu k}}{dt} \quad (31)$$

Applying the direct and inverse Concordia transformation to the triphase system defined by (31) implies:

$$\frac{d}{dt}\begin{bmatrix} i_{\mu\alpha} \\ i_{\mu\beta} \end{bmatrix} = C_{23}\begin{bmatrix} h_1 & 0 & 0 \\ 0 & h_2 & 0 \\ 0 & 0 & h_3 \end{bmatrix} * C_{32}\frac{d}{dt}\begin{bmatrix} \varphi_{\mu\alpha} \\ \varphi_{\mu\beta} \end{bmatrix} \quad (32)$$

Where h_k can be defined

$$h_k = h(i_{\mu k}, \varphi_{\mu k}, i_{\mu k}) \quad (33)$$

By substituting (14), (15), (19), and (20) in the vector equation (32), one constructs the two following sixth and seventh state space equations of the AC machine:

$$\frac{di_{\mu\alpha}}{dt} = \frac{1}{6}(4h_1 + h_2 + h_3)(V_{r\alpha} - R_r i_{\mu\alpha} + R_r i_{s\alpha} - \omega\varphi_{r\beta}) - \frac{\sqrt{3}}{6}(h_2 - h_3)(V_{r\beta} - R_r i_{\mu\beta} + R_r i_{s\beta} - \omega\varphi_{r\alpha}) \quad (34)$$

$$\frac{di_{\mu\beta}}{dt} = -\frac{\sqrt{3}}{6}(h_2 - h_3)(V_{r\alpha} - R_r i_{\mu\alpha} + R_r i_{s\alpha} - \omega\varphi_{r\beta}) + \frac{1}{2}(h_2 + h_3)(V_{r\beta} - R_r i_{\mu\beta} + R_r i_{s\beta} - \omega\varphi_{r\alpha}) \quad (35)$$

Equations (19), (20), (23), (24), (27), (34), and (35) represent the established DFIG state space model. For a more compact form, let's consider the following state space model:

$$\dot{X} = F(X) + G\,u \tag{36}$$

$$y = \lambda(X) = \begin{bmatrix} \Omega \\ \varphi_{r\alpha}^2 + \varphi_{r\beta}^2 \end{bmatrix} \tag{37}$$

with

$$X = \left[i_{s\alpha}, i_{s\beta}, \varphi_{r\alpha}, \varphi_{r\beta}, \Omega, i_{\mu\alpha}, i_{\mu\beta}\right]^T \tag{38}$$

$$u = \left[V_{r\alpha}, V_{r\beta}\right]^T \tag{39}$$

$$G = \begin{bmatrix} -\frac{1}{L_s} & 0 & 1 & 0 & 0 & 0 & 0 \\ 0 & -\frac{1}{L_s} & 0 & 1 & 0 & 0 & 0 \end{bmatrix}^T \tag{40}$$

$$F(X) = \begin{bmatrix} -\frac{R_s}{L_s} i_{s\alpha} + \frac{1}{L_s} V_{s\alpha} - \frac{1}{L_s}\left[-R_r i_{\mu\alpha} + R_r i_{s\alpha} - \omega\varphi_{r\beta}\right] \\ -\frac{R_s}{L_s} i_{s\beta} + \frac{1}{L_s} V_{s\beta} - \frac{1}{L_s}\left[-R_r i_{\mu\beta} + R_r i_{s\beta} + \omega\varphi_{r\alpha}\right] \\ -R_r i_{\mu\alpha} + R_r i_{s\alpha} - \omega\varphi_{r\beta} \\ -R_r i_{\mu\beta} + R_r i_{s\beta} + \omega\varphi_{r\alpha} \\ \frac{P}{J}\left(\varphi_{r\alpha} i_{s\beta} - \varphi_{r\beta} i_{s\alpha}\right) - \frac{T_L}{J} \\ f_6(X) \\ f_7(X) \end{bmatrix} \tag{41}$$

with

$$f_6(X) = \frac{1}{6}(4h_1 + h_2 + h_3)\left(V_{r\alpha} - R_r i_{\mu\alpha} + R_r i_{s\alpha} - \omega\varphi_{r\beta}\right) - \frac{\sqrt{3}}{6}(h_2 - h_3)\left(V_{r\beta} - R_r i_{\mu\beta} + R_r i_{s\beta} - \omega\varphi_{r\alpha}\right) \tag{42}$$

$$f_7(X) = -\frac{\sqrt{3}}{6}(h_2 - h_3)\left(V_{r\alpha} - R_r i_{\mu\alpha} + R_r i_{s\alpha} - \omega\varphi_{r\beta}\right) + \frac{1}{2}(h_2 + h_3)\left(V_{r\beta} - R_r i_{\mu\beta} + R_r i_{s\beta} - \omega\varphi_{r\alpha}\right) \tag{43}$$

4. SPEED AND FLUX CONTROLLER DESIGN AND ANALYSIS

Any control strategy for DFIG is characterized by two main components:

a) The rotor flux reference generator used
b) The DFIG model was considered during the design of the regulator.

In this context, Depending on the way these components are designed four control strategies are considered (see Table-2).

Table-2. Different speed control strategies.

		Reference Flux generator	
		Nominal Flux	**Optimal Flux**
Magnetic Characteristic model	Linear	LMC-NF	LMC-OF
	Hysteretic	HMC-NF	HMC-OF

In the existing literature, the most popular DFIG control strategy is the LMC-NF which is characterized by a non-optimal constant flux reference and an MPPT controller designed from the linear magnetic model. There, the constant flux reference should normally be given the machine flux nominal value. The resulting control performances are not satisfactory from an energetic viewpoint, especially in the presence of small wind speeds.

The LMC-OF control strategy is characterized by a variable flux reference, this latter is computed considering for each torque value the minimal stator current, the main interest of this configuration is to minimize the joule losses in the stator, and this will allow the extraction of more power from the generator. The speed regulator is designed considering a linear hysteretic magnetic characteristic.

The HMC-NF control strategy (see Table-2) is characterized by a constant flux set point. The speed regulator is designed taking into account the hysteretic magnetic characteristic. Such a strategy is practically useless as no benefit is gained from model complexity if the flux reference is kept constant.

The present paper focuses on the new control strategy (HMC-OF) that consists in designing an optimal flux reference generator and an MPPT controller (Figure-5). The latter is designed based on the non linear model (36)–(43) that takes into account the hysteretic feature of the DFIG magnetic characteristic. The flux reference optimality is expected to guarantee the minimization of the stator current required to produce the maximum electromagnetic torque corresponding to a given wind speed. The proposed control strategy is presented in detail in Subsections 4.1 and 4.2.

4.1 Optimal Speed Reference and Flux Reference Generator

4.1.1 Optimal flux reference computing

The conception of the optimal flux reference algorithm consists in presenting the optimal stator current in the function of the rotor flux for each

VOL. 18, NO. 7, APRIL 2023 ISSN 1819-6608
ARPN Journal of Engineering and Applied Sciences

www.arpnjournals.com

value of the mechanical torque. To this end, representing the mechanical torque in a d-q reference frame seems to be more interesting from a computing point of view.

If we orient the d component of the reference frame following the rotor flux, the flux q-component is null and all state variables are constant in steady-state. Since $\varphi_{rq} = 0$ the torque equation becomes

$$T_m = p\varphi_r i_{sq} \tag{44}$$

From (23)-(24), the d-q components of the stator voltages in a steady state are given by

$$V_{sd} = R_s i_{sd} - \omega_s \varphi_{sq} \tag{45}$$

$$V_{sq} = R_s i_{sq} + \omega_s \varphi_{sd} \tag{46}$$

Substituting (12)-(13) in (45)-(46), one has

$$V_{sd} = R_s i_{sd} - l_s \omega_s i_{sq} \tag{47}$$

$$V_{sq} = R_s i_{sq} + \omega_s (l_s i_{sd} + \varphi_r) \tag{48}$$

The stator's direct connection to the grid leads one to the following equality:

$$V_{smax}^2 = V_{sd}^2 + V_{sq}^2 \tag{49}$$

By substituting (47) and (48) in (49) one has:

$$V_{smax}^2 = [R_s^2 + l_s^2\omega_s^2] i_{sd}^2 + 2\omega_s l_s \varphi_r i_{sd} + [l_s^2\omega_s^2 + R_s^2] i_{sq}^2 + 2R_s\omega_s\varphi_r i_{sq} + \omega_s^2\varphi_r^2 \tag{50}$$

By introducing (44) in (50) the d component of the stator current verify

$$i_{sd} = -\frac{\omega_s l_s \varphi_r}{[R_s^2+l_s^2\omega_s^2]} + \sqrt{\left[\frac{\omega_s l_s \varphi_r}{[R_s^2+l_s^2\omega_s^2]}\right]^2 + \frac{V_{smax}^2}{[R_s^2+l_s^2\omega_s^2]} - \left(\frac{T_m}{p\varphi_r}\right)^2 - \frac{2R_s\omega_s\varphi_r}{[R_s^2+l_s^2\omega_s^2]}\frac{T_m}{p\varphi_r} - \frac{\omega_s^2}{[R_s^2+l_s^2\omega_s^2]}\varphi_r^2} \tag{51}$$

let's consider I_s the norm of the stator current, then using (50) and (58), the resulting norm of the stator current could be given by

$$I_s = \sqrt{{i_{sd}}^2 + {i_{sq}}^2} \tag{52}$$

$$I_s = \sqrt{\left[-\frac{\omega_s l_s \varphi_r}{[R_s^2+l_s^2\omega_s^2]} + \sqrt{\left[\frac{\omega_s l_s \varphi_r}{[R_s^2+l_s^2\omega_s^2]}\right]^2 + \frac{V_{smax}^2}{[R_s^2+l_s^2\omega_s^2]} - \left(\frac{T_m}{p\varphi_r}\right)^2 - \frac{2R_s\omega_s\varphi_r}{[R_s^2+l_s^2\omega_s^2]}\frac{T_m}{p\varphi_r} - \frac{\omega_s^2}{[R_s^2+l_s^2\omega_s^2]}\varphi_r^2}\right]^2 + \sqrt{\left[\frac{T_m}{p\varphi_r}\right]^2}} \tag{53}$$

Equation (53) expresses I_s as a function of T_m and φ_r.

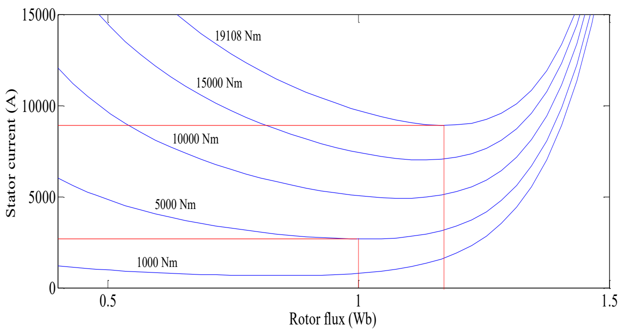

Figure-3. Curves of torque (19108, 15000, 10000, 5000, and 1000Nm) each curve design a current minimum corresponding to the optimal flux.

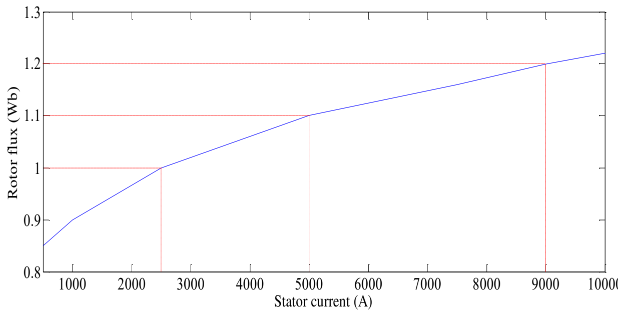

Figure-4. Optimal current–flux (OCF) characteristic.

A sample of 9 relevant torque values T_{m_j} (j=1,…,9) has been a priori selected and the corresponding global minima $(\varphi^*_{T_{m_j}}, I^*_{T_{m_j}})$ can be graphically determined as illustrated by Figure-4 where all the curves correspond to the induction machine characterized by the numerical parameters of Table-3. Doing so, a set of 9 global minima $(\varphi^*_{T_{m_j}}, I^*_{T_{m_j}})$ (j=1,…,9) has been obtained. The set of minima points have been fitted in the least squares sense by a polynomial function of nth-order, denoted F(.). The degree n=5 proved to be suitable for the data under consideration. The polynomial created in this manner is denoted by:

ARPN Journal of Engineering and Applied Sciences

$$F(I_s) = \theta_n I_s^n + \theta_{n-1} I_s^{n-1} + \cdots + \theta_1 I_s + \theta_0 \quad (54)$$

Table-3. Coefficients of the polynomial F(.).

Index	Value	Index	Value	Index	Value
θ_0	0.85	θ_1	−0.061	θ_2	0.4986
θ_3	−1.71	θ_4	3.1370	θ_5	−2.838

4.1.2 Optimal speed reference

The main interest of working under a variable speed reference is that the choice of this reference can be made optimal to extract the maximum available power. Furthermore, the achievement of this latter guarantees optimal aerodynamic efficiency.

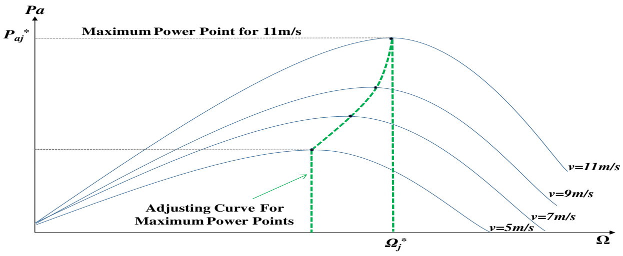

Figure-5. The shape of the aerodynamic power according to the rotor speed for various values of wind speed. Highlighting MPP.

For a given wind speed, there exists a unique optimal rotor speed reference for extracting the maximum mechanical power (see Fig.5). For this, a sample of 20 relevant wind speed values v_j ($j = 1, \ldots, 20$) has been a priori selected and the corresponding global maxima (Ω_j^*, P_{aj}^*) can be graphically determined [11]. By doing so, a set of 20 points $(\Omega_{rj}^*, P_{aj}^*)$ ($j = 1, \ldots, 20$) has been constructed. Then, a n[th]-order polynomial function *R(.)*, fitting in the least squares sense the set of $(\Omega_{rj}^*, P_{aj}^*)$ points, has been built. For the considered wind turbine, characterized by the numerical parameters of Table-2 and the shape of $C_P(\lambda)$ presented in [11], the degree $n = 4$ turned out to be convenient for the considered data. The polynomial thus constructed is denoted:

$$R(v) = w_4 v^4 + w_3 v^3 + w_2 v^2 + w_1 v + w_0 \quad (55)$$

where the coefficients w_j have the numerical values of Table-4. For the considered wind system, the shape of $R(v)$ is plotted in Figure-6 which will be referred to as an optimal wind speed power (OWRS) characteristic.

Table-4. Numerical values of coefficients in the polynomial R(v).

Index	Value	Index	Value	Index	Value
w_0	45	w_2	9.996	w_4	−0.002
w_1	−0.04247	w_3	0.064		

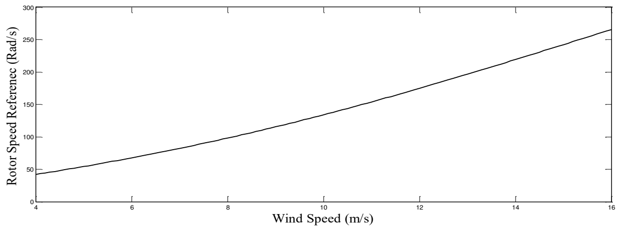

Figure-6. Optimal wind-rotor speed (OWRS) characteristic.

4.2 Rotor Speed and Rotor Flux Controller Design Analysis

We are interested in the problem of controlling the rotor speed and flux norm for the doubly fed induction generator described by the model (36-43) that takes into account, the saturation and hysteresis of the magnetic characteristic. The speed and flux references (Ω_{ref},φ_{ref}) are any bounded and derivable functions of time and their two first derivatives are available and bounded. These conditions can always comply with filtering the reference through second-order linear filters.

The controller design will now be performed in two steps using the backstepping technique. First, let's introduce the tracking errors:

$$e_1 = \Omega_{ref} - \Omega \quad (56)$$

$$z_1 = \varphi_{ref}^2 - \left(\varphi_{r\alpha}^2 + \varphi_{r\beta}^2\right) \quad (57)$$

Step 1: It follows from (36)-(43) that the errors e_1 and z_1 undergo the following differential equations:

$$\dot{e}_1 = \dot{\Omega}_{ref} - \frac{P}{J}\left(\varphi_{r\alpha} i_{s\beta} - \varphi_{r\beta} i_{s\alpha}\right) + \frac{T_L}{J} \quad (58)$$

$$\dot{z}_1 = 2\varphi_{ref}\dot{\varphi}_{ref} - 2\varphi_{r\alpha}\dot{\varphi}_{r\alpha} - 2\varphi_{r\beta}\dot{\varphi}_{r\beta} \quad (59)$$

By substituting (19)-(20) in (59) one has:

$$\dot{z}_1 = 2\varphi_{ref}\dot{\varphi}_{ref} - 2\varphi_{r\alpha}V_{r\alpha} - 2\varphi_{r\beta}V_{r\beta} + 2R_r\left(\varphi_{r\alpha} i_{\mu\alpha} + \varphi_{r\beta} i_{\mu\beta}\right) - 2R_r\left(\varphi_{r\alpha} i_{s\alpha} + \varphi_{r\beta} i_{s\beta}\right) \quad (60)$$

In equations (58) the quantities $\mu_1 = \frac{P}{J}\left(\varphi_{r\alpha} i_{s\beta} - \varphi_{r\beta} i_{s\alpha}\right)$ stand up as virtual control signal. So that, for the tracking error e_1 vanishes asymptotically, let us consider the following virtual control:

$$\mu_1 = c_1 e_1 + \dot{\Omega}_{ref} + \frac{T_L}{J} \quad (61)$$

Similarly, to control the tracking error z_1, equation (60) suggests choosing the quantity $2\varphi_{r\alpha}V_{r\alpha} + 2\varphi_{r\beta}V_{r\beta}$ (considered as a virtual control) such that:

$$2\varphi_{r\alpha}V_{r\alpha} + 2\varphi_{r\beta}V_{r\beta} = d_1 z_1 + 2\varphi_{ref}\dot{\varphi}_{ref} + 2R_r\left(\varphi_{r\alpha} i_{\mu\alpha} + \varphi_{r\beta} i_{\mu\beta}\right) - 2R_r\left(\varphi_{r\alpha} i_{s\alpha} + \varphi_{r\beta} i_{s\beta}\right) \quad (62)$$

ARPN Journal of Engineering and Applied Sciences

where c_1 and d_1 are any positive real design parameters. Indeed, let's consider the Lyapunov's candidate function defined by:

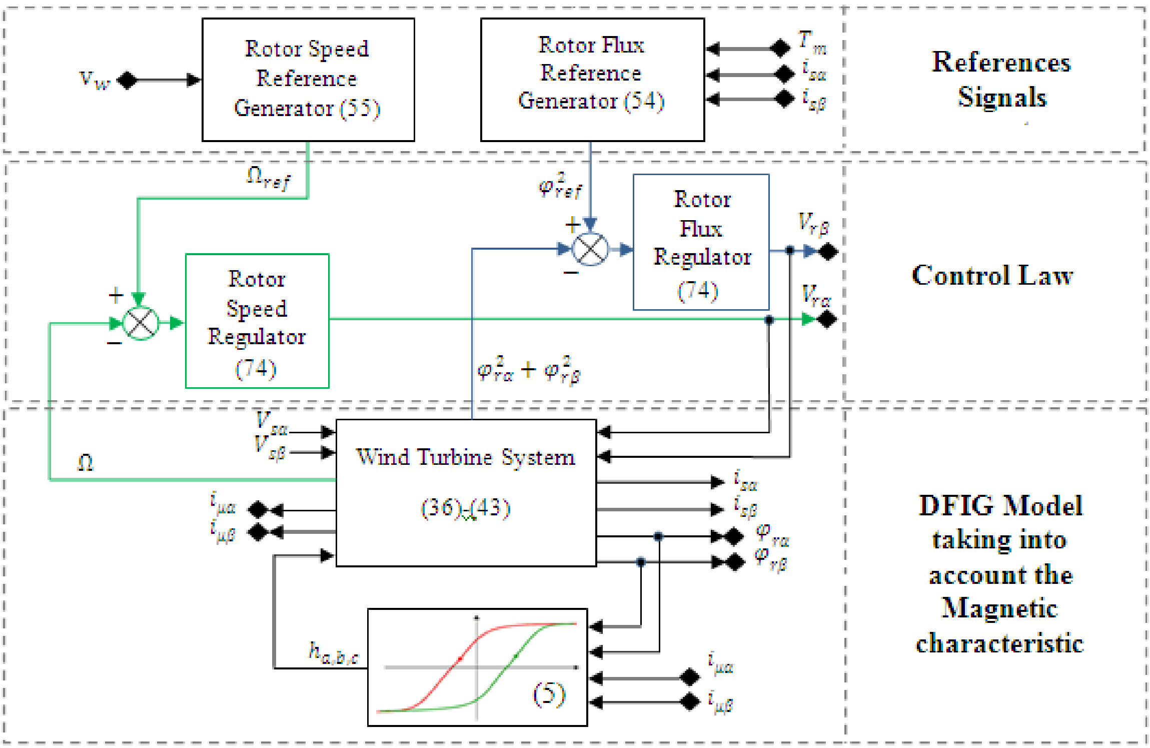

Figure-7. Control loops of the whole studied system.

$$V_1 = \frac{1}{2}(e_1^2 + z_1^2) \tag{63}$$

Its time derivative is given by (using (61)-(62))

$$\dot{V}_1 = -c_1 e_1^2 - d_1 z_1^2 \tag{64}$$

In this step, μ_1 is retained as a first stabilization function, and the new tracking errors denoted $e_2$is defined:

$$e_2 = \mu_1 - \frac{P}{J}\left(\varphi_{r\alpha} i_{s\beta} - \varphi_{r\beta} i_{s\alpha}\right) \tag{65}$$

By substituting (61) in (65), the tracking error $e_1$dynamic is given by

$$\dot{e}_1 = -c_1 e_1 + e_2 \tag{66}$$

Consequently, the time derivative of Lyapunov's candidate function (63) becomes:

$$\dot{V}_1 = -c_1 e_1^2 - d_1 z_1^2 + e_1 e_2 \tag{67}$$

Step 2: The second step consists in choosing the actual control signals, $V_{r\alpha}$ and $V_{r\beta}$, so that all error vectors $[e_1, z_1, e_2]^T$ converge to zero. The time derivative of the tracking error e_2 is given by:

$$\dot{e}_2 = \dot{\mu}_1 - \frac{P}{J}\left(\dot{\varphi}_{r\alpha} i_{s\beta} + \varphi_{r\alpha}\dot{i}_{s\beta} - \dot{\varphi}_{r\beta} i_{s\alpha} - \varphi_{r\beta}\dot{i}_{s\alpha}\right) \tag{68}$$

By substituting (36)-(43) and (61) in (68) one has:

$$\dot{e}_2 = \mu_2 - \frac{P}{J}\left(V_{r\alpha} i_{s\beta} - \frac{1}{L_s} V_{r\beta}\varphi_{r\alpha} - V_{r\beta} i_{s\alpha} + \frac{1}{L_s} V_{r\alpha}\varphi_{r\beta}\right) \tag{69}$$

where

$$\mu_2 = 2c_1(c_1 e_1 + e_2) + \ddot{\Omega}_{ref} + \frac{\dot{T}_L}{J} - \frac{P}{J}\Big(-R_r i_{\mu\alpha} i_{s\beta} + R_r i_{s\alpha} i_{s\beta} - \omega\varphi_{r\beta} i_{s\beta} - \frac{R_s}{L_s}\varphi_{r\alpha} i_{s\beta} + \frac{1}{L_s} V_{s\beta}\varphi_{r\alpha} + \frac{R_r}{L_s} i_{\mu\beta}\varphi_{r\alpha} - \frac{R_r}{L_s} i_{s\beta}\varphi_{r\alpha} - \frac{1}{L_s}\omega\varphi_{r\alpha}^2 + R_r i_{\mu\beta} i_{s\alpha} - R_r i_{s\beta} i_{s\alpha} - \omega\varphi_{r\alpha} i_{s\alpha} + \frac{R_s}{L_s}\varphi_{r\beta} i_{s\alpha} - \frac{1}{L_s} V_{s\alpha}\varphi_{r\beta} - \frac{R_r}{L_s}\varphi_{r\beta} i_{\mu\alpha} + \frac{R_r}{L_s}\varphi_{r\beta} i_{s\alpha} - \frac{1}{L_s}\omega_r\varphi_{r\beta}^2 - \frac{1}{L_s}\left(V_{s\alpha}\varphi_{r\beta} - V_{s\beta}\varphi_{r\alpha}\right)\Big) \tag{70}$$

To analyze the error system (e_1, z_1, e_2) stability, let us consider the following extended Lyapunov function candidate:

$$V_2 = V_1 + \frac{1}{2} e_2^2 \tag{71}$$

Its time-derivative along the trajectory of the state vector (e_1, z_1, e_2) is given by (using (67) and (69)):

ISSN 1819-6608
ARPN Journal of Engineering and Applied Sciences

$$\dot{V}_2 = -c_1 e_1^2 - d_1 z_1^2 + e_2\left(e_1 + \mu_2 - \frac{P}{J}\left(V_{r\alpha}\left(i_{s\beta} + \frac{1}{L_s}\varphi_{r\beta}\right) - V_{r\beta}\left(i_{s\alpha} - \frac{1}{L_s}\varphi_{r\alpha}\right)\right)\right) \quad (72)$$

To ensure the global and asymptotic stability of the error system, the control inputs $V_{r\alpha}, V_{r\beta}$ should be chosen as the following:

$$e_2\left[e_1 + \mu_2 - \frac{P}{J}\left(V_{r\alpha}\left(i_{s\beta} + \frac{1}{L_s}\varphi_{r\beta}\right) - V_{r\beta}\left(i_{s\alpha} - \frac{1}{L_s}\varphi_{r\alpha}\right)\right)\right] = -c_2 e_2^2 \quad (73)$$

Where c_2 is a positive design parameter? Then, using (62) and (73), one has:

$$\begin{bmatrix} V_{r\alpha} \\ V_{r\beta} \end{bmatrix} = \begin{bmatrix} \left(i_{s\beta} + \frac{1}{L_s}\varphi_{r\beta}\right) & -\left(i_{s\alpha} - \frac{1}{L_s}\varphi_{r\alpha}\right) \\ 2\varphi_{r\alpha} & 2\varphi_{r\beta} \end{bmatrix}^{-1} \cdot \begin{bmatrix} \frac{J}{P}(c_2 e_2 + e_1 + \mu_2) \\ d_1 z_1^2 + 2\varphi_{ref}\dot{\varphi}_{ref} + 2R_r(\varphi_{r\alpha} i_{\mu\alpha} + \varphi_{r\beta} i_{\mu\beta}) - 2R_r(\varphi_{r\alpha} i_{s\alpha} + \varphi_{r\beta} i_{s\beta}) \end{bmatrix} \quad (74)$$

Theorem 1 (Main result)

Consider the closed-loop system composed of the DFIG, described by the model (36)-(43) and the nonlinear controller defined by the control law (74). The closed-loop error system described by (e_1, z_1, e_2) respectively given in (56, 57, and 65) is globally asymptotically stable concerning the Lyapunov function (72). Consequently, all errors vanish exponentially fast, whatever the initial conditions☐

Proof of Theorem 1

With the proposed control laws defined in (74), the time derivative of the considered Lyapunov's function (71) is given by:

$$\dot{V}_2 = -c_1 e_1^2 - d_1 z_1^2 - c_2 e_2^2 \quad (75)$$

As $\dot{V}_2$ is a negative definite function of the state vector (e_1, z_1, e_2), the error system is globally asymptotically stable. This completes the proof of Theorem 1■

5. SIMULATIONS RESULTS

The simulation was performed in Matlab/Simulink environment. The performances of the proposed new controller, (that accounts for the magnetic hysteresis) will be evaluated through several tests of robustness. In the next this controller will be referred to as HMC-OF. To highlight the supremacy of the HMC-OF, three comparisons will be performed: the first test involves control strategies with state-dependent optimal flux reference over control strategies with a nominal constant flux reference (see Table-2). The second test is to prove the HMC-OF performances compared to the standard controller assuming that the DFIG magnetic characteristic is linear (in the next this controller will be referred to as LMC-NF), this latter is working under a nominal flux reference. The last test will include a comparison between the HMC-OF and the LMC-OF, both controllers are working under optimal flux reference, but the second is based on a linear flux magnetic characteristic. The considered DFIG is a 3MW whose characteristics are summarized in Table-4. The new controller design parameters are in Table-5, and the standard controller parameters are in Table-6.

Table-5. Electrical machine parameters.

Electrical	Index	Value
Stator/Rotor resistance	Rs/ Rr	0.455/0.62Ω
S/Rotor leakage inductance	Ls/ Lr	0.0083/0.0081H
Magnetizing inductance	Msr	0.0078H
Inertia	J	0.3125kgm2
Viscous friction	F	6.73×10−1Nms−1

Table-6. New controller parameters.

Index	Value
C1	450
C2	240
d_1	5000

5.1 Simulation Protocol

The simulation protocol is set up to take into account a significant step variation in the mean wind speed, as illustrated in Figure-. The algorithms used to calculate the rotor flux and rotor speed references are discussed in subsections 4.1.2 and 4.1.1, respectively.

Many grid faults will be applied to the HMC-OF to assess its robustness. To prove its good behaviour facing real grid operation mode. These tests are classified into two parts: robustness under voltage dips and robustness despite the frequency variation. The first considered fault is a 3-phase voltage dip, which reduces the main voltage value by about 60% and last for 1s [4s-5s] as presented in Figure-9a. The second test was carried out by considering a frequency variation [50-50.5 Hz]. This grid fault is introduced at time 1s and last for 0.5s as shown in Figure-9b.

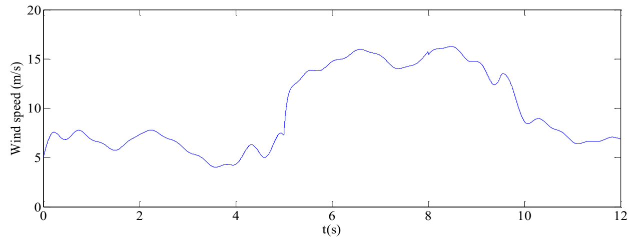

Figure-8. Wind speed is considered profile.

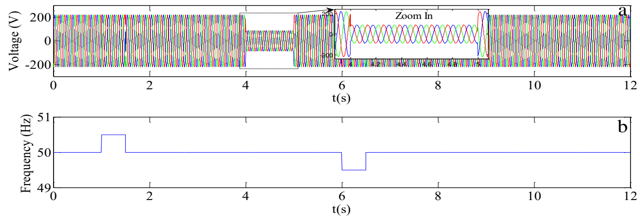

Figure-9a. Network voltage under voltage dips. Fig.9b. Network frequency profile.

5.2 Controller Evaluation

a) Supremacy of the HMC-OF strategy over the HMC-NF strategy (Table-2)

The HMC-OF is implemented using equation (74). The corresponding design parameters are given by the numerical values of Table-3. Figure-10 illustrates that the HMC-OF as well as the HMC-NF track well the given speed reference, both are computed using the curve of the optimal rotor speed (see Figure-3) ensuring the MPPT objective. However, the HMC-OF delivers more precision and presents fewer oscillations than the HMC-NF. Furthermore, Figure-10 highlights the good robustness of the proposed HMC-OF in the presence of the considered grid faults (described in Figures 9a-9b), where it is clearly shown that the faults don't affect the tracking objectives.

Similarly, Figure-11 and Figure-12 present respectively the HMC-OF and HMC-NF rotor flux tracking performances. This figure illustrates the good behavior of the proposed regulators even under the considered voltage dips and frequency deviation. Note that in Figure-11 the considered flux reference is variable in function of the stator current to optimize the joule losses in the stator (see subsection 4.1.1). While in Figure-12 the flux reference considered is constant in the order of 1.1wb (equal to the nominal flux).

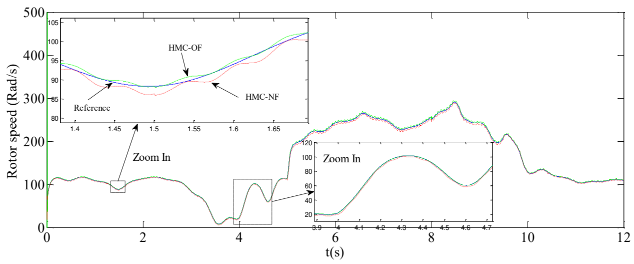

Figure-10. Speed tracking performance of HMC-OF. Solid: speed reference. Dotted: HMC-NF speed response. Dashed line: HMC-OF.

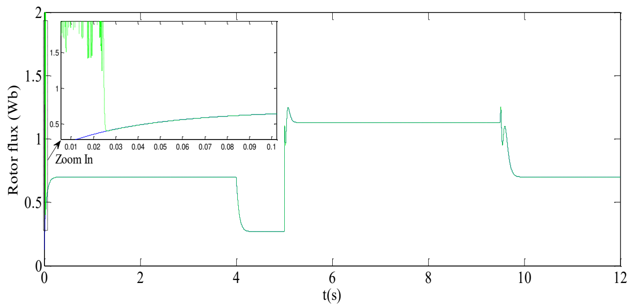

Figure-11. Rotor flux tracking performances. Solid line: Rotor flux reference. Dotted line: HMC-OF.

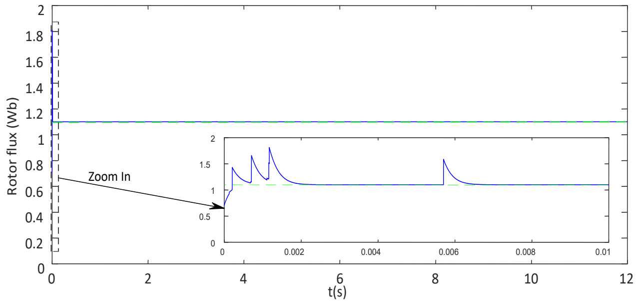

Figure-12. Rotor flux tracking performances. Solid line: Rotor nominal flux reference. Dotted line: HMC-NF.

Since the difference between the HMC-OF and the HMC-NF is in the rotor flux level, it is imperial to proceed to a power comparison to judge the interest of one on the other, for that, a power comparison is realized, between the power extracted from the generator working with the HMC-OF, and the power extracted from the generator working with the HMC-NF, note that both power computing systems are considering the hysteresis/saturation phenomena. Figure-13 shows clearly that the power with the optimal flux reference (Solid line) is greater than the power with the steady flux reference (Dotted line), proving that with the optimal rotor flux, the joule losses of power are less, and the produced power is greater. Around 12% more power is collected using the optimal flux reference for the selected wind profile, attesting to the benefits of this controller.

The joule losses are obtained considering the expression $\frac{3}{2}R_S I_S^2$, where I_s is the norm of the stator current. Figure-14 presents the evolution of these losses for both controllers HMC-OF and HMC-NF, it is clearly shown that the HMC-OF implies lower losses than the HMC-NF, especially for weak values of the wind speed. This achieves the comparison between the HMC-OF and the HMC-NF.

ISSN 1819-6608
ARPN Journal of Engineering and Applied Sciences

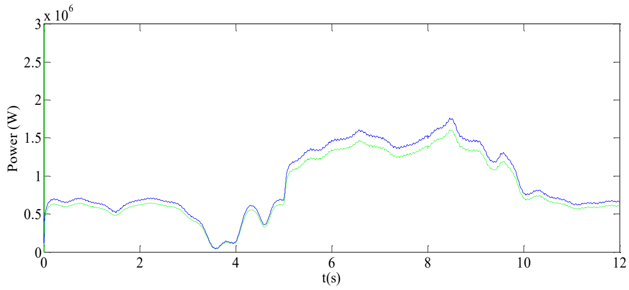

Figure-13. Extracted power comparison. Dotted line: HMC-NF. Solid line: HMC-OF.

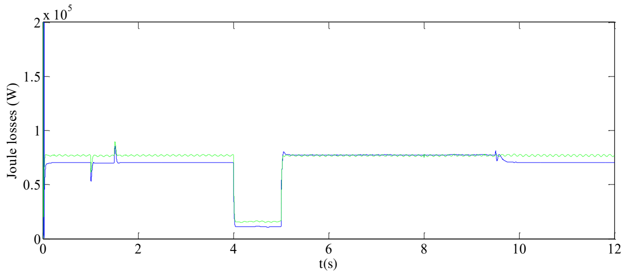

Figure-14. Joule losses power. Dotted line: HMC-NF Solid line: HMC-OF.

b) Supremacy of the HMC-OF strategy over the LMC-NF strategy

In this subsection the LMC-NF involving nominal flux reference is considered for a comparison purpose, the controller is obtained simply by considering (31):

- the function h constant and equals h=250, this is obtained by studying the linearization of the hysteresis shape of Figure-2.
- the flux reference constant and equal to 1.1Wb
- and the other design parameters with the following values that proved to be convenient for this controller: C_1=1200, C_2=420, d_1=100.

Figure-15 presents the rotor speed tracking by the HMC-OF and by the LMC-NF, it attests clearly to the good response of the HMC-OF tracking the speed reference. On the other hand, the LMC-NF presents some imprecision in low rotor speeds, once the speed rises the tracking performances of the LMC-NF improves. Figure-16 attests that the LMC-NF ensures the tracking of the rotor flux reference. However, small oscillations appear for different values of wind speed.

Note that the simulation process of the LMC-NF working with the machine taking the hysteresis/saturation phenomena into account did take great effort and time to deliver such results, in other words no better results could be achieved with this configuration.

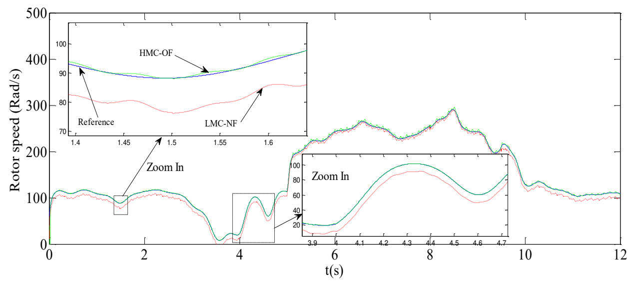

Figure-15. Speed tracking performance of LMC-NF. Solid: speed reference. Dotted: LMC-NF speed response. Dashed line: HMC-OF.

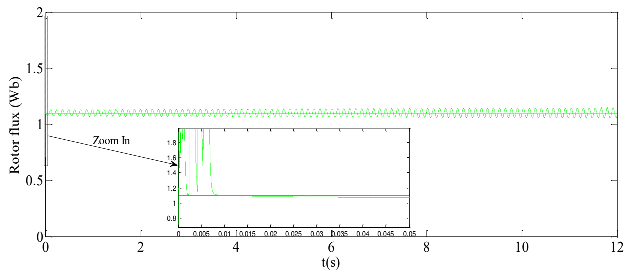

Figure-16. Rotor flux tracking performances. Solid line: Rotor flux reference. Dotted line LMC-NF.

To complete the proof of the great interest of the HMC-OF, a power analyze was performed in Figure-17. The solid line presents the power delivered by the wind turbine working with the HMC-OF, where the power is proved maximal since we are operating in MPPT mode. The dotted line presents the power delivered by the wind turbine controlled by the LMC-NF. One can note that there is a power gap from the power delivered by the HMC-OF. This analysis proves that with the HMC-OF working under real phenomena, one can extract more power than with the standard regulator, in low and high wind speeds.

It is well seen in Figure-18 that the HMC-OF involves smaller joule losses compared to the LMC-NF. This achieves the comparison between the HMC-OF and the LMC-NF.

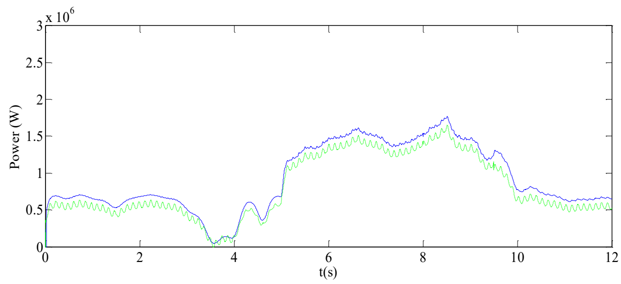

Figure-17. Extracted power comparison. Dotted line: LMC-NF. Solid line: HMC-OF.

ARPN Journal of Engineering and Applied Sciences

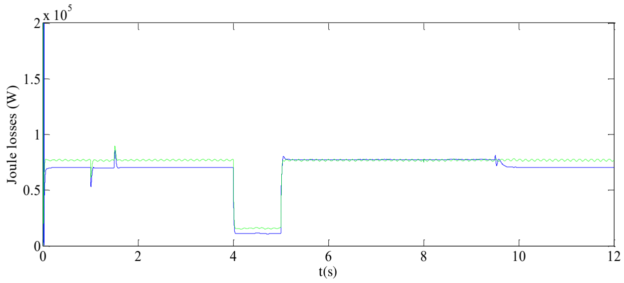

Figure-18. Joule losses power. Dotted line: LMC-NF. Solid line: HMC-OF.

c) Supremacy of the HMC-OF strategy over the LMC-OF strategy

The LMC-OF has the exact shape of the LMC-NF, except that:

- The flux reference is delivered by the optimal flux reference generator (see subsection 4.1.1)
- The controller parameters are given the following values that proved to be convenient: C_1=450, C_2=240, d_1=100.

Figure-19 presents the rotor speed tracking performances, of both HMC-OF and LMC-NF. It is well seen that the HMC-OF gives more precision, especially in low wind speeds operating mode. Once the speed rises, the tracking performance of the LMC-OF improves.

Figure-20 shows the rotor flux tracking performances of the LMC-OF. Where one can attest that the tracking is ensured around the nominal rotor flux value, and not ensured with great accuracy elsewhere.

The power comparison of the HMC-OF over the LMC-OF attests that with the first controller, more power is extracted, especially in low wind speeds operating mode as presented in Figure-21.

It is well seen in Figure-22 that the HMC-OF involves smaller joule losses compared to the LMC-OF. This achieves the comparison between the HMC-OF and the LMC-OF.

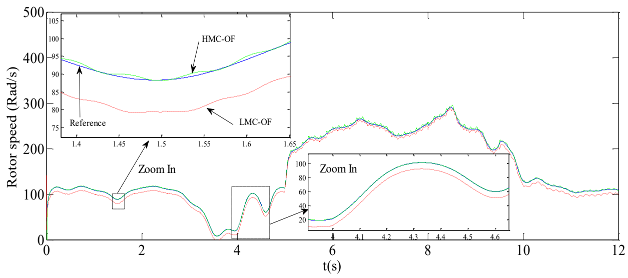

Figure-19. Speed tracking performance of LMC-OF. Solid: speed reference. Dotted: LMC-NF speed response. Dashed line: HMC-OF

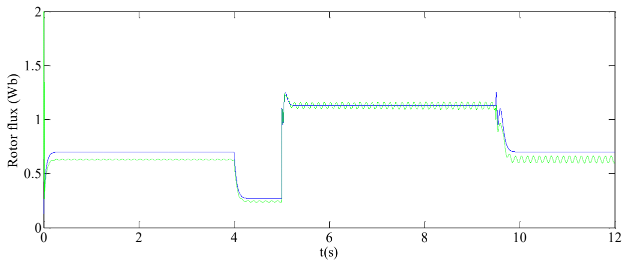

Figure-20. Rotor flux tracking performances. Solid line: Rotor flux reference. Dotted line LMC-OF.

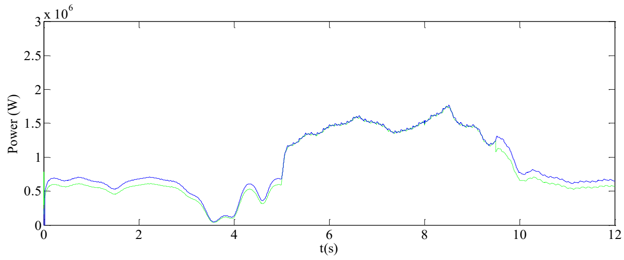

Figure-21. Extracted power comparison. Dotted line: LMC-OF. Solid line: HMC-OF.

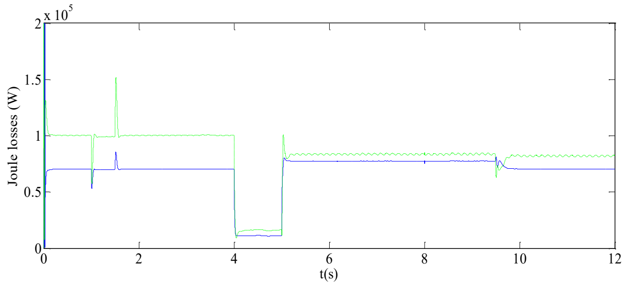

Figure-22. Joule losses power. Dotted line: LMC-OF. Solid line: HMC-OF.

6. CONCLUSIONS

In this paper, we proposed a nonlinear controller for the doubly fed induction generator operating in the presence of magnetic characteristic saturation and hysteresis. The control purpose was to regulate the rotor speed and the rotor flux. The references of these latter are delivered respectively by an optimal rotor speed reference generator, consumed to deliver a speed reference corresponding to the maximum available power, and an optimal rotor flux reference algorithm, performed to help this machine consume less power by the joule affects in the stator, and by that to generate more power. For this, The HMC-OF described by (74) has been designed using the backstepping technique, based on the model defined in (36-43). Theorem 1 formally establishes the global convergence of the errors $e_1 = \Omega_{ref} - \Omega$ and $z_1 = \varphi_{ref}^2 - (\varphi_{r\alpha}^2 + \varphi_{r\beta}^2)$ to zero. The controller was analyzed to determine sufficient conditions to track well the given references. It is proved that both errors vanish whatever the operating conditions. The system's global stability was studied and proved by the Lyapunov's theory. These theoretical results were confirmed by simulations on

ARPN Journal of Engineering and Applied Sciences

Matlab/Simulink environment involving a wide range variation of the wind speed. The robustness of the new controller was also evaluated through several tests. Indeed, this allowed checking that the new controller maintains its good performances despite a grid frequency variation or under voltage dips.

REFERENCES

[1] Ouadi H., Giri F., Elfadili A., Dorleans P. and Massieu J. F. 2010. Induction Machine Control in Presence of Magnetic hysteresis Modelling and Speed reference tracking. IFAC Proceedings Volumes. 43(10): 7-12.

[2] Coleman B. D., M. L. Hodgdon. 1987. On a class of constitutive relations for ferromagnetic hysteresis. Arch. Rational Mech. Anal. pp. 375-396.

[3] Du, J., Feng. Y., Su, C. Y., and Hu, Y. M. 2009. On the robust control of systems preceded by coleman-hodgdon hysteresis. In IEEE 2009 Internatinal conference on control and automation (pp 685-689). IEEE.

[4] Voros J. 2009. Modeling and identification of hysteresis using special forms of the Coleman-Hodgdon model. J. Electr. Eng. 60(2) : 100-105.

[5] Chen X., Hisayama T. and Su C. Y. 2008, December. Adaptive control for continuous-time systems preceded by hysteresis. In Decision and Control, 2008. CDC 2008. 47th IEEE Conference on (pp. 1931-1936). IEEE.

[6] El Fadili A., Giri F., El Magri A., Lajouad R., Chaoui F. 2013. Adaptive control strategy with flux reference optimization for sensorless induction motors. Control Engineering Practice. 26(May 2014): 91-106.

[7] Akel F., Ghennam T., Berkouk E. M., Laour M. 2014. An improved sensorless decoupled power control scheme of grid connected variable speed wind turbine generator. Energy Conversion and Management. 78: 584-594.

[8] Sarrias-Mena Raúl., Fernández-Ramírez L. M., García-Vázquez C. A., Jurado F. 2014. Fuzzy logic based power management strategy of a multi-MW doubly-fed induction generator wind turbine with battery and ultra-capacitor. Energy. 70: 561-576.

[9] Dida A., Benattous D. 2015. Modeling and control of DFIG through back-to-back five levels converters based on neuro-fuzzy controller. Journal of Control, Automation and Electrical Systems. 26(5): 506-520.

[10] Hamane B., Benghanem M., Bouzid M. A., Belabbes A., Bouhamida M., Draou A. 2012. Control for Variable Speed Wind Turbine Driving a Doubly Fed Induction Generator using Fuzzy-PI Control. Energy Procedia. 18: 476-485.

[11] Barra A., Ouadi H., Giri F. 2016. Sensorless Nonlinear Control of Wind Energy Systems with Doubly Fed Induction Generator. Journal of control, Automation and Electrical Systems. 27(5): 562-578.

[12] Ouadi H., Giri F., Elfadili A. and Dugard L. 2010. Induction machine speed control with flux optimization. Control Engineering Practice. 18(1): 55-66.

[13] El fadili A., Giri F., Ouadi H., Dugard L. and El Magri, A. 2009, August. Induction machine control in presence of magnetic saturation speed regulation with optimized flux reference. In Control Conference (ECC), 2009 European (pp. 2542-2547). IEEE.

[14] Macki Jack W., Paolo Nistri and Pietro Zecca. 1993. Mathematical models for hysteresis. SIAM review. 35.1: 94-123.

[15] Ouadi H., Barra A. and El Majdoub K. 2017. Nonlinear control for grid connected wind energy system with multilevel inverter. ARPN Journal of Engineering and Applied Sciences. 12(4).